ICSO 2016

International Conference on Space Optics

Biarritz, France

18–21 October 2016

Edited by Bruno Cugny, Nikos Karafolas and Zoran Sodnik

Low-order aberration coefficients applied to design of telescopes with freeform surfaces

Bryan D. Stone

Joseph M. Howard

esa icso proceedings cnes

International Conference on Space Optics — ICSO 2016, edited by Bruno Cugny, Nikos Karafolas, Zoran Sodnik, Proc. of SPIE Vol. 10562, 1056229 · © 2016 ESA and CNES
CCC code: 0277-786X/17/$18 · doi: 10.1117/12.2296163

LOW-ORDER ABERRATION COEFFICIENTS APPLIED TO DESIGN OF TELESCOPES WITH FREEFORM SURFACES

Bryan D. Stone[1], Joseph M. Howard[2]

[1]*Synopsys, Inc., USA.*
377 Simarano Drive
Marlborough, MA 01753
bryans@synopsys.com

[2]*NASA Goddard Space Flight Center, USA*
Code 551, Optics Branch
Greenbelt, MD 20771
joseph.m.howard@nasa.gov

I. INTRODUCTION

As the number of smallsats and cubesats continues to increase [1], so does the interest in the space optics community to miniaturize reflective optical instrumentation for these smaller platforms. Applications of smallsats are typically for the Earth observing community, but recently opportunities for them are being made available for planetary science, heliophysics and astrophysics concepts [2]. With the smaller satellite platforms come reduced instrument sizes that they accommodate, but the specifications such as field of view and working f/# imposed on the smaller optical systems are often the same, or even more challenging. To meet them, and to "fit in the box", it is necessary to employ additional degrees of freedom to the optical design. An effective strategy to reduce package size is to remove rotational symmetry constraints on the system layout, allowing it to minimize the unused volume by applying rigid body tilts and decenters to mirrors. Requirements for faster systems and wider fields of view can be addressed by allowing optical surfaces to become "freeform" in shape, essentially removing rotational symmetry constraints on the mirrors themselves. This dual approach not only can reduce package size, but also can allow for increased fields of view with improved image quality.

Tools were developed in the 1990s to compute low-order coefficients of the imaging properties of asymmetric tilted and decentered systems [3][4]. That approach was then applied to reflective systems with plane symmetry, where the coefficients were used to create closed-form constraints to reduce the number of degrees of freedom of the design space confronting the designer [5][6]. In this paper we describe the geometric interpretation of these coefficients for systems with a plane of symmetry, and discuss some insights that follow for the design of systems without closed-form constraints. We use a common three-mirror design form example to help illustrate these concepts, and incorporate freeform surfaces for each mirror shape.

In section II, we evoke the typical form of the wave aberration function taught in most texts on geometrical optics, and then recast it into a general form that no longer assumes rotational symmetry. A freeform surface definition for mirrors is then defined, and the example three-mirror system used throughout this paper is introduced. In section III, the first-order coefficients of the plane symmetric system are discussed, and then the second-order in section IV. In both of these discussions, the example system is perturbed to present the explicit form of the aberration coefficient laid out in section II, and plots are presented using optical design software. Finally, some concluding remarks are given in section V.

II. PRELIMINARIES

By way of introduction, consider the wave aberration function for a rotationally-symmetric system:

$$\begin{aligned} W(h,\boldsymbol{\rho}) = \; & w_d\,\boldsymbol{\rho}^2 && \leftarrow \text{First Order} \\ & + w_1\,\boldsymbol{\rho}^4 + w_2\,h\rho_y\rho^2 + w_3\left(h\rho_y\right)^2 + w_4\,h^2\boldsymbol{\rho}^2 + w_5\,h^3\rho_y && \leftarrow \text{Third order} \\ & + O(5), && \leftarrow \text{Higher Order (odd only)} \end{aligned} \tag{1}$$

where h is the normalized object coordinate (taken, without loss of generality, to lie along the Y-axis in the object space), $\boldsymbol{\rho} = (\rho_x, \rho_y)$ is the normalized pupil coordinate, $\boldsymbol{\rho}^2 = (\rho_x^2 + \rho_y^2)$, w_d represents defocus from the paraxial image, and w_1 through w_5 are the conventional third-order aberration coefficients [7].

Two things to note: 1) The "order" of the aberrations are traditionally based on the transverse ray error, which is proportional to the derivative of the wave aberration function with respect to the pupil coordinates. Thus, the so-called "third" order aberrations are actually of degree "four" in the wave aberration function. 2) The even order terms all vanish for rotationally symmetric systems on account of the symmetry.

For a symmetric system, the wave aberration function represents a Taylor expansion of the imaging properties about the axial ray. When symmetry is broken, it is natural to consider a Taylor expansion about the ray that

starts at the center of the object and passes through the center of the aperture stop. Such a ray is referred to here as the Base Ray for the system. In this paper we consider the low-order terms of such an expansion and discuss the associated imaging properties. This discussion is not entirely general, however. We specialize to the case of systems where the system possesses a plane of symmetry and the base ray lies in that plane. In this work, the *Y-Z* plane is taken to be the plane of symmetry. Under these assumptions, the wave aberration function (through second-order) can be written as follows [8].

$$\begin{aligned} W(\boldsymbol{h},\boldsymbol{\rho}) = {} & \tfrac{1}{2}\left(w_{dx}\rho_x^2 + w_{dy}\rho_y^2\right) && \leftarrow \text{First Order} \\ & + \tfrac{1}{2}B_{112}\,\rho_x^2\rho_y + \tfrac{1}{6}B_{222}\,\rho_y^3 && \leftarrow \text{Second Order; Constant over Field} \\ & + N_{112}\,h_x\rho_x\rho_y + \tfrac{1}{2}N_{211}\,h_y\rho_x^2 + \tfrac{1}{2}N_{222}\,h_y\rho_y^2 && \leftarrow \text{Second Order; Linear in Field} \\ & + \tfrac{1}{2}L_{112}\,h_x^2\rho_y + L_{211}\,h_xh_y\rho_x + \tfrac{1}{2}L_{222}\,h_y^2\rho_y && \leftarrow \text{Second Order Distortion} \\ & + O(3), && \leftarrow \text{Higher Order (even + odd)} \end{aligned} \quad (2)$$

Where (h_x, h_y) are the normalized object coordinates. The notation is chosen to be consistent with the work in [4]. The form of this equation follows solely from the requirement of symmetry about the *Y-Z* plane and there are no other assumptions built into Eq. (2).

Note that there is one piece that is important in the context of first-order optics is missing from the wave-aberration function: focal length. In this work we assume the object at infinity, so we exclusively discuss focal length, but the concepts associated with magnification are very similar when the object is finite.

The goal of this paper is to describe these first and second order properties that occur once symmetry is broken, and to discuss considerations that are relevant in the context of freeform designs. In order to facilitate that discussion, a well-corrected, three-mirror system is now introduced. This design is derived from a three-mirror sample lens that is shipped with CODE V® [9] that originally started with two conic mirrors and a third rotationally symmetric more general aspheric mirror. The final design used in this paper has a focal length of 420mm, a 4-degree square full field-of-view, and operates at F/4.

The design was modified so that the mirrors are all free-form surfaces represented as an *X-Y* polynomial whose sag equation is given by:

$$\mathrm{Z} = \frac{c\,r^2}{1+\sqrt{1-c^2(\kappa+1)r^2}} + \sum_{i,j} C_{i,j}\,x^i\,y^j \quad (3)$$

where (x, y) are coordinates on the surface, $r^2 = (x^2+y^2)$, c and κ are the curvature and conic constant of the base conic, and the $C_{i,j}$ are the coefficients of the aspheric polynomial. As an aside, note that other surface representations such as Zernike or Forbes freeform [10] could have been used, but we needed only relatively low-order aspheres (two mirrors are fifth-order polynomials, and one is sixth-order), and the direct connection between polynomial terms and the derivatives of the surface profile made the use of the *X-Y* polynomial particularly convenient for this work. Because the system is symmetric about the *Y-Z* plane, only the terms that have even powers of x are non-zero (i.e., the $C_{i,j}$ are taken to be zero for odd i). Without loss of generality, the vertex of each mirror is placed at the point of intersection of the mirror with the base ray. For systems with conic mirrors, say, the ability to move the base ray off the vertex of the mirror can be an important degree of freedom, but for freeform mirrors it is not necessary to move the mirror vertex off the base ray; any arbitrary surface profile can be realized without utilizing such a degree of freedom. The system was optimized after converting the mirrors to such freeform surfaces by allowing only the coefficients in the mirror profiles ($C_{i,j}$) to vary (and no other system parameters like distance between mirrors or mirror tilts).

As expected, the extra degrees of freedom afforded by the X-Y polynomial allow the system to improve beyond the starting design form and diffraction-limited performance was obtained (wavelength of 500nm). A cross-sectional view of the system and the resulting MTF is shown in Fig. 1. This system is referred to as the "Sample System" in the remainder of this work, and it is used extensively in the discussion that follows, sometimes with further modifications of aspheric coefficients of the mirrors in order to vary a single (or set of) aberration coefficient(s). A CODE V macro was written in which the first- and second-order coefficients in the wave aberration function [Eq. (2)] are computed, so that these coefficients could be constrained to be given values during optimization. These constraints are imposed primarily for illustrative purposes in this paper, but in most practices the coefficients would be constrained to be zero. In the next two sections, each of the terms appearing in Eq. (2) is discussed in more detail.

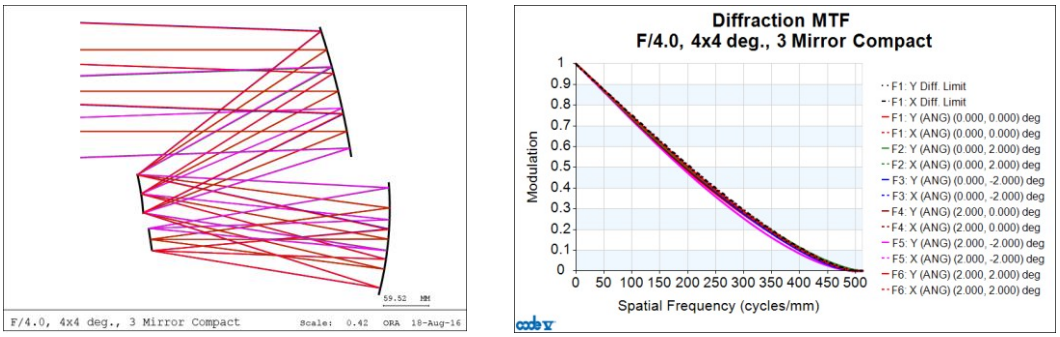

Fig. 1. A cross-sectional view of the Sample System (left) and the MTF of the Sample System (right)

III. FIRST ORDER

A. Focus (basal astigmatism)

Conventional, symmetric optical systems, have a single focal point. However, once symmetry is broken it follows from Eq. (2) that there are generally two focal points (when w_{dx} and w_{dy} are unequal). For a system with plane-symmetry, a fan of rays closely spaced about the base ray in the *Y-Z* plane focus at one focal point, and a fan that is perpendicular to the *Y-Z* plane focuses at another. This is illustrated schematically in the left-hand portion of Fig. 2.

The Sample System introduced in the previous section was initially optimized with constraints that ensure these two focal points coincide, but now, for illustrative purposes, we use a constraint during optimization to force these focal points apart while allowing only the quadratic terms in the mirror profiles to vary. Following such optimization, the separation between the focal points is 0.1 mm and one can observe vertical line images (parallel to the *Y*-axis) on the original image plane, and horizontal line images on a plane shifted by 0.1mm; the medial image lies half-way in between. This is illustrated by the spot diagrams shown in the right-hand portion of Fig. 2. Note that unlike conventional 3rd order astigmatism, this form of first-order astigmatism is constant over the field.

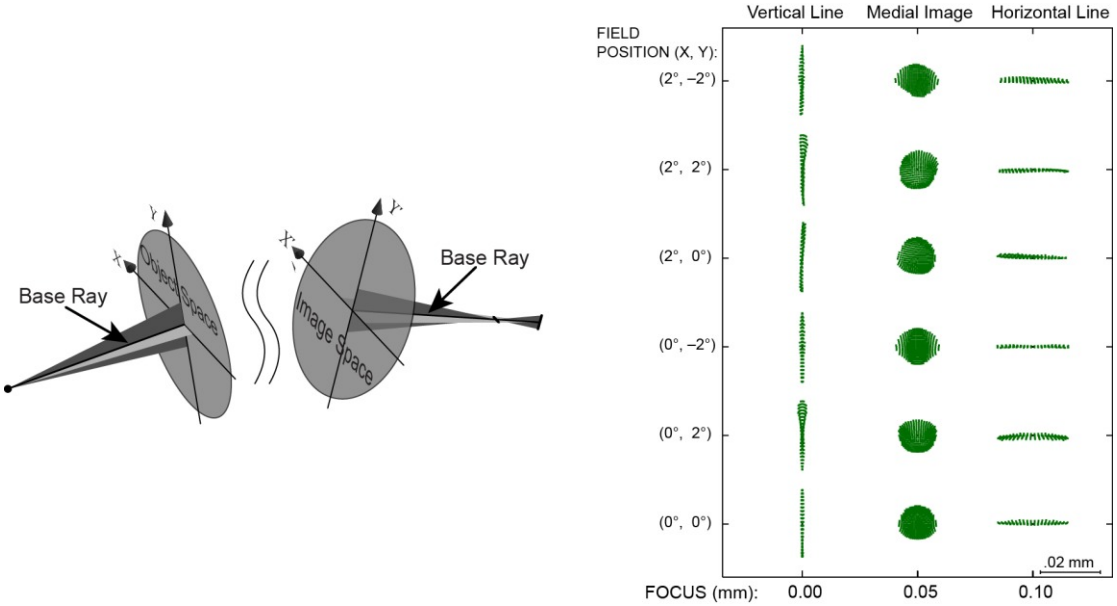

Fig. 2. A schematic representation of basal astigmatism (left); The spot diagrams for the Sample System when the focal points are constrained to have a separation of 0.1mm (right).

B. Focal Length (Anamorphic imagery)

The focal length generalizes in a manner similar to the focal point: there are two distinct focal lengths, one in the *X*-direction and one in *Y*. As illustrated schematically in the left-hand portion of Fig. 3, a square object is generally imaged to a rectangle, where the ratio of the lengths of the sides of the rectangle equals the ratio of the principal focal lengths in *X* and *Y* (denoted by f_x and f_y). When the initial optimization was performed for the

Sample System, constraints were used to ensure that the focal lengths are equal to each other and to the desired value of 420mm. However, the focal lengths need not be the same and in order to illustrate this effect, the Sample System was re-optimized with the X-focal length constrained to 440mm and the Y-focal length constrained to 400mm. As illustrated in the right-hand portion of Fig. 3, a square object is mapped to a rectangular image (as represented by the solid lines), whereas if both focal lengths are set equal to 420 mm (as was done originally for the Sample System), the square object is mapped to a square image (dashed lines).

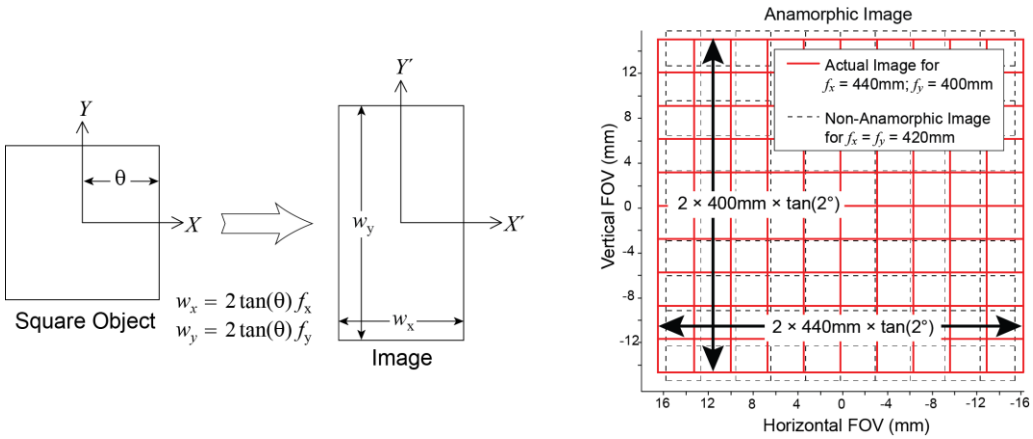

Fig. 3. A schematic representation of anamorphic imagery (left); The distortion grid for the Sample System when constrained to have different focal lengths in the *X*- and *Y*-directions (right).

The terms of second-order in the wave aberration function are discussed in the following section.

IV. SECOND ORDER

A. Terms Constant Over Field: $\frac{1}{2}B_{112}\,\rho_x^2\rho_y + \frac{1}{6}B_{222}\,\rho_y^3$

These terms are independent of field, and in this sense are analogs of spherical aberration. However, the aperture dependence differs significantly from conventional third-order spherical. In what follows, it is useful also to consider the transverse ray errors. The transverse ray errors, denoted here as $(\varepsilon_x, \varepsilon_y)$, are proportional to the derivatives [with respect to the pupil coordinates, (ρ_x, ρ_y)] of the wave aberration function [Eq. (2)]:

$$\varepsilon_x \propto B_{112}\rho_x\rho_y\,, \tag{4a}$$

$$\varepsilon_y \propto \frac{1}{2}B_{112}\rho_x^2 + \frac{1}{2}B_{222}\rho_y^2\,. \tag{4b}$$

It follows from these equations that for B_{112}, a circle of rays in the pupil (centered on the base ray) are mapped to an ellipse on the image. Every such ellipse contains the point of intersection of the base ray with the image, and therefore the geometric point spread function is brightest at the base ray and gets dimmer as one moves away from the base ray. B_{222} gives a line image, but it is a very different wavefront than one gets with astigmatism (cubic as opposed to quadratic) so the through-focus behavior, while not shown here, is very different than one sees for conventional astigmatism. The image of a set of points on the object is shown schematically in Fig. 4.

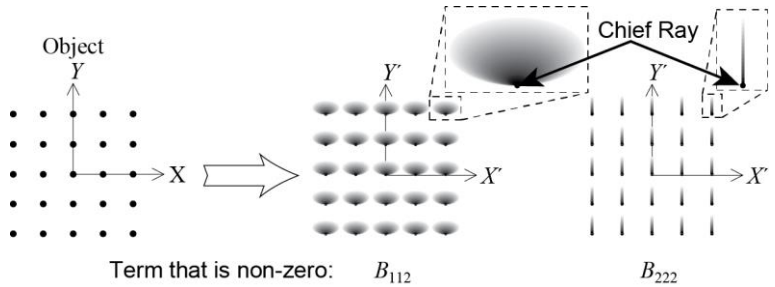

Fig. 4. Schematic illustration of the imagery associated with second order terms that are constant over field.

If we take the Sample System and now constrain it to possess only B_{112} (through second order), or separately only B_{222}, we get spot diagrams as shown in Fig. 5 (left and center). The diffraction point-spread-function is

also shown for each of the field points. The intensity in the point spread function (PSF) is represented on a logarithmic scale. There are some high-order pieces that cause the PSF to not be precisely constant with field, but the spot diagram and diffraction point-spread-functions are nonetheless easily recognizable as being dominated over the field by each of the respective terms. Note, however, that it is not common to see a system dominated by just one of these two terms. For example, when $B_{222} = 3\ B_{112}$, the resulting PSFs look like classical, 3rd order coma, but it is constant over the field. This scenario is familiar from nominally rotationally symmetric systems that are misaligned, but it can also be seen more generally. Such a case is illustrated in the right-hand portion of Fig. 5, where the Sample System is constrained to possess the given ratio of B_{112} to B_{222}.

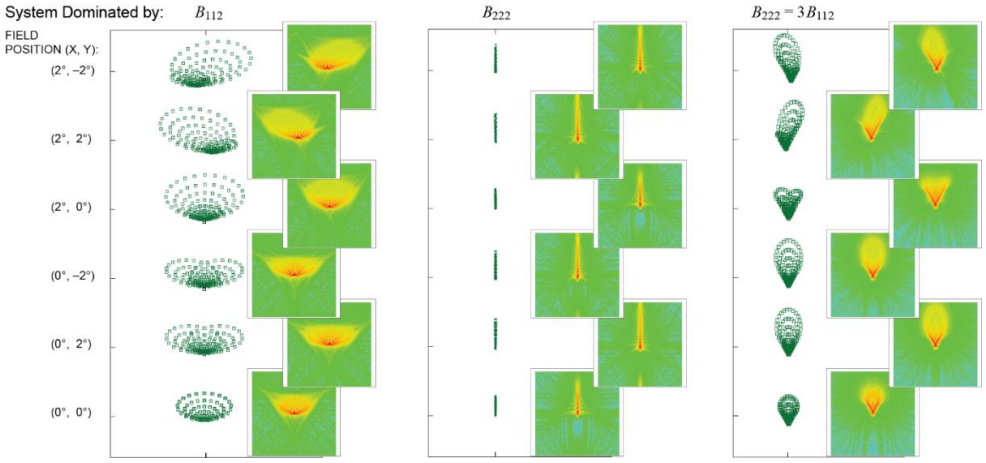

Fig. 5. Spot diagrams and diffraction point-spread-function for the Sample System constrained to be dominated by one of B_{112} (left), B_{222} (center), or a combination where $B_{222} = 3\ B_{112}$ (right).

B. Terms Linear in the Field: $N_{112}\ h_x\rho_x\rho_y + \frac{1}{2}N_{211}\ h_y\rho_x^2 + \frac{1}{2}N_{222}\ h_y\rho_y^2$

These terms vary linearly with field coordinate and are quadratic in the pupil. The transverse ray aberrations associated with these terms are shown below.

$$\varepsilon_x \propto N_{112}h_x\rho_y + N_{211}h_y\rho_x\ , \tag{5a}$$
$$\varepsilon_y \propto N_{112}h_x\rho_x + N_{222}h_y\rho_y\ . \tag{5b}$$

It is seen that these terms all represent astigmatic wavefronts. For N_{112}, the astigmatic line images are oriented at 45°; the image plane lies on the medial image and the aberration grows linearly with the *Y*-coordinate of the field. N_{211} and N_{222} are closely related to each other and represent astigmatism that gives either horizontal line images (for $N_{211} \neq 0$) or vertical line images (for $N_{222} \neq 0$) that grow linearly with the X-coordinate. The images associated with a grid of points on the object are represented schematically in Fig. 6.

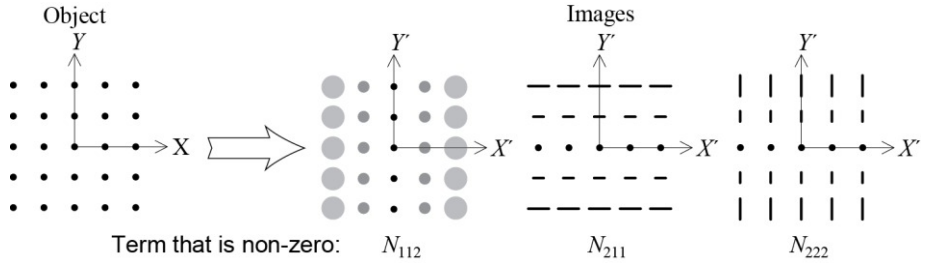

Fig. 6. Schematic illustration of the imagery associated with second order terms that are linear in the field.

The image plane tilt affects N_{112} only weakly, but both N_{211} and N_{222} are roughly linear in the tangent of the image tilt, so it can be used to switch between having horizontal or vertical line images. If the image plane tilt is chosen to lie in between those planes that give the vertical and horizontal line images (that is, on the medial image), then it will occur that $N_{211} = -N_{222}$ and the point spread function is roughly circular. The two image planes on which vertical (green) or horizontal (red) line images occur are illustrated schematically in the right-hand portion of Fig. 7. In the left-hand portion of Fig. 7, the spot diagrams for three different image tilts are shown for the Sample System when it is constrained to possess only N_{211}/N_{222}. Notice that along the *X*-axis (*Y*-angle of 0°), the spot diagrams are very small and do not change significantly over this range of image tilt. For

the field points with the *Y*-angle equal to ± 2°, the spot diagrams are approximately constant, and by varying the tilt of the image, horizontal line, circular, or vertical line images result for these field points.

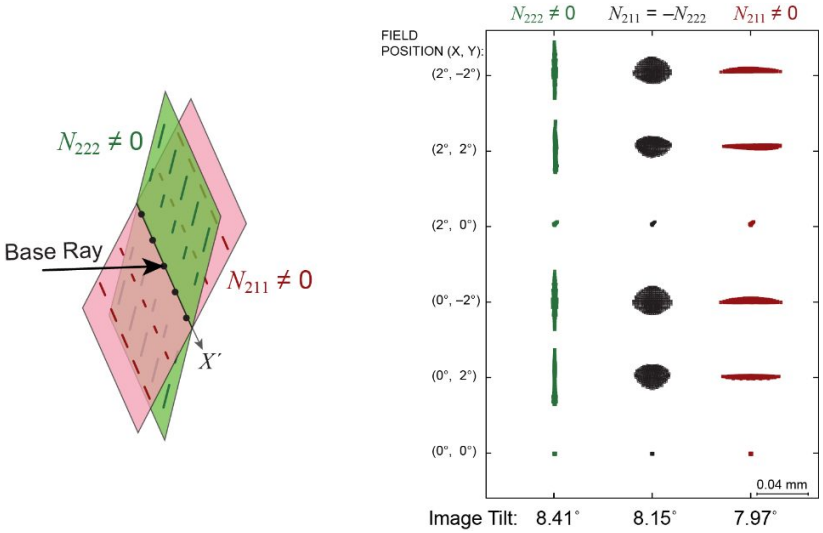

Fig. 7. Schematic illustration of the change in the image as the image plane is tilted (left); Spot diagrams for three different tilts of the image plane for the Sample System when constrained to possess only N_{112}/N_{222} (right).

In order to reinforce these ideas, the Sample System as modified for the spot diagrams in the right-hand portion of Fig. 7 is analyzed and the geometric RMS spot diameter computed over a grid of points in the field. The results are shown in the left-hand portion of Fig. 8. In that figure, the size of the diameter of each circle is proportional to the spot size at the corresponding field point. It is seen that, as expected, the blur is linear in the *Y*-coordinate of the field. The insets in the figure represent the wavefront error for four select field points to emphasize that the aberrations are dominated by astigmatism aligned to the plane of symmetry, but that the astigmatism has opposite signs on opposite sides of the *X*-axis.

Next, the Sample System is re-optimized with the N_{112} term constrained to be non-zero. The central portion of Fig. 8 represents the variation of the geometric RMS spot size over the field. It is seen that the blur is linear in the X-coordinate of the field. The wavefront errors shown for three fields emphasize that the aberrations are dominated by astigmatism oriented at 45 degrees.

Similar to the terms that are independent of field, it is not common for a system to be dominated by just one of these terms. More typically, they appear in combination as is shown in the right-hand portion of Fig. 8. It is seen that the spot size grows linearly with the distance from the center of the field. The wavefront error for some select field points are shown and it is seen that the orientation of the astigmatism varies as one moves around the center of the field.

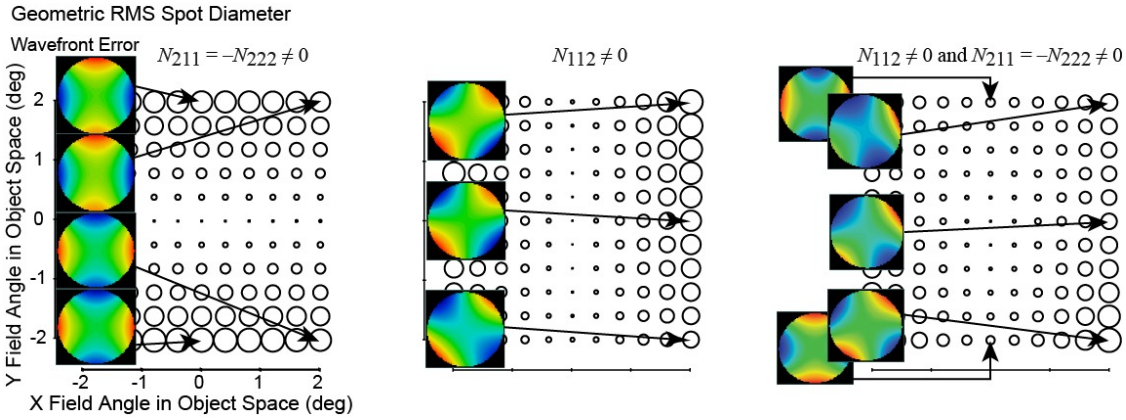

Fig. 8. On each of these plots, the size of the circle is proportional to the geometric RMS spot size. The insets represent the wavefront error for a few select field points. For the plot on the left, the performance is shown for the medial image plane for the case where N_{211}/N_{222} are non-zero. In the central plot, the system is dominated by N_{112}. The right-most plot is for a system with a mixture of both $N_{112,}$ and N_{211}/N_{222}.

C. Distortion terms: $\frac{1}{2}L_{112}\,h_x^2\rho_y + L_{211}\,h_x h_y \rho_x + \frac{1}{2}L_{222}\,h_y^2\rho_y$

These terms do not introduce blur; they represent distortion and as such the transverse ray error given in Eqs. (6) are independent of the pupil coordinate. It follows from these equations that the forms of the distortion associated with each of the individual coefficients is as shown in Fig. 9. As an aside, note that L_{211}, L_{222}, and anamorphic magnification are the primary components of classic keystone distortion.

$$\varepsilon_x \propto L_{211}\,h_x h_y \tag{6a}$$
$$\varepsilon_y \propto \tfrac{1}{2}L_{112}\,h_x^2 + \tfrac{1}{2}L_{222}\,h_y^2 \tag{6b}$$

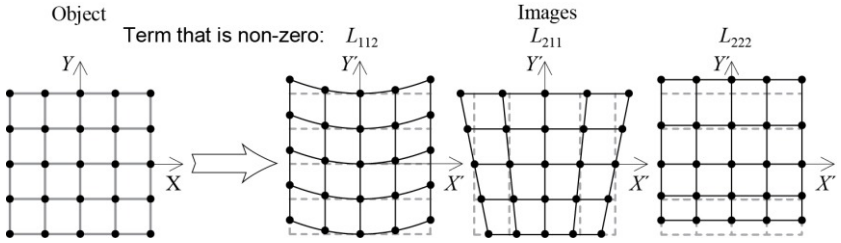

Fig. 9. Schematic illustration of the distortion represented by the three second-order distortion terms.

The Sample System had no constraints on distortion when it was optimized for this paper. The distortion in the original lens is shown in the upper portion of Fig. 10 on the left. It is seen that this system is dominated by L_{222}, with some lesser amount of L_{112}. The system was re-optimized and an attempt was made to control the coefficients of 2nd order distortion. If only the mirror aspheric coefficients are allowed to vary, the distortion can be reduced, as seen in the center column of Fig. 10. In this case, there are significant contributions to the distortion from all three second-order distortion terms. Note, however, that the reduced distortion comes at the cost image quality (as demonstrated by the MTF curves below the distortion plots). If the mirror locations and tilts are allowed to vary as well as the aspheric coefficients, the distortion can be corrected to a much higher degree without any degradation in the imaging performance (as demonstrated by the right-hand portion of Fig. 10). Because we were only controlling the second-order coefficients of distortion, the residual distortion is seen to be higher order, but additional constraints could be added to the optimization to further reduce this residual distortion (but that was not done here). Cross-sectional views of the system before and after optimization are shown in the insets of Fig. 10.

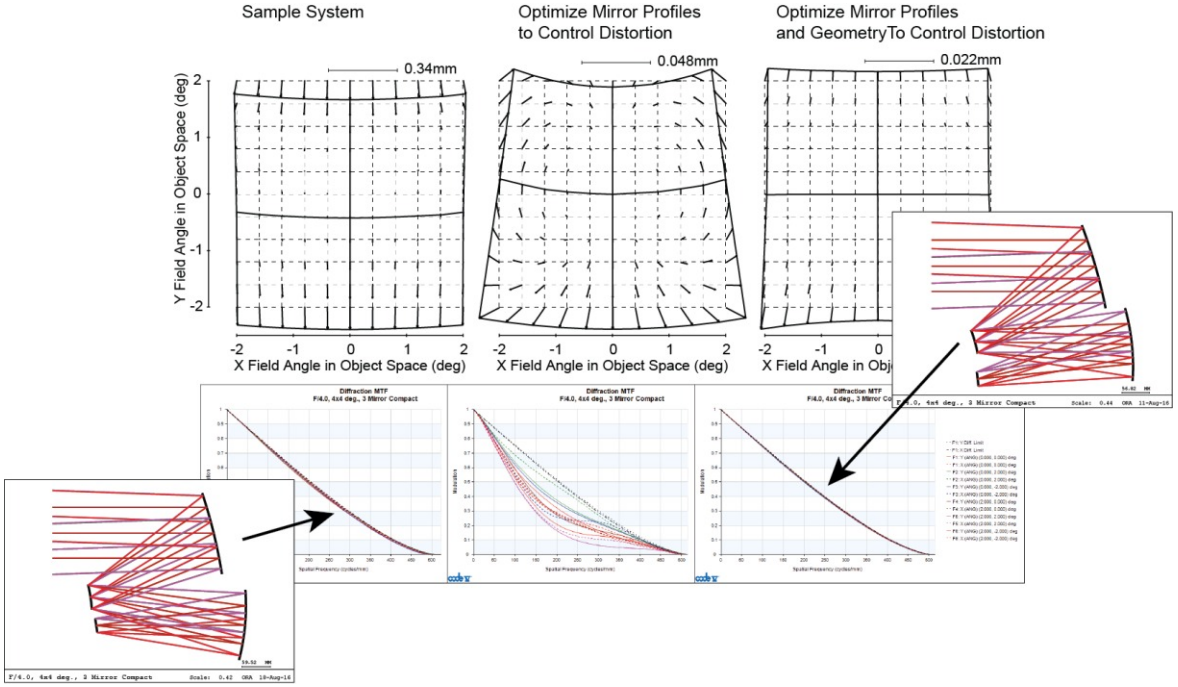

Fig. 10. The top row represents distortion plots for the Sample System (left), the Sample System re-optimized to control distortion but varying only aspheric coefficients (center), and the Sample System re-optimized to control distortion but varying both aspheric coefficients and mirror tilts and separations (right). The associated MTF plots are also shown, and cross-sectional plots of the lenses appear in the insets.

V. CONCLUDING REMARKS

In this paper we have described imaging properties associated with the first- and second-order aberrations for plane-symmetric systems. In previous work, we explicitly built constraints that ensure desired values for these coefficients for spherical mirror systems and systems with conic mirrors [5][6]. However, rather than surrendering degrees of freedom explicitly, here we compute the aberration coefficients and formulate optimization constraints from them. The constraint-handling of the optimizer is used to ensure given values for these low-order coefficients. Even when letting the constraint handling of the optimizer "do the work", it is nonetheless useful to have some understanding, in the context of freeform optics, of the degrees of freedom that can effectively control these coefficients. Akin to a fourth-order aspheric coefficient in relation to conventional third-order aberrations, it is useful to identify, those variables for which an aberration coefficient is linear (or nearly so). In principal such linear variables can be solved in closed form to ensure that the associated aberration coefficient takes a given value, but even when letting the optimizer handle this, we know that variables that give linear changes in a constraint are particularly effective when used during optimization.

As a concrete example, the first-order properties (basal astigmatism and focal lengths) are linear in the second derivative of the surface at the point where it intersects the base ray. Therefore, to constrain a system to possess given focal lengths and to require the basal astigmatism be zero, one can surrender three degrees of freedom: $C_{2,0}$ and $C_{0,2}$, [i.e., the coefficients of x^2 and y^2 in Eq. (3)] on one mirror, and either $C_{2,0}$ or $C_{0,2}$ on another. If the first-order image location is to be prescribed, a fourth degree of freedom can also be surrendered. Having these coefficients be variable during the optimization allows these constraints to be held effectively.

It is shown in [4] that the second-order coefficients, B_{112}, N_{112}, N_{211}, L_{112}, L_{211} are all linear in the $C_{2,1}$ term on each mirror [i.e., the coefficient of $x^2\,y$ in Eq. (3)], while B_{222}, N_{222}, and L_{222} are linear in $C_{0,3}$ (the coefficient of y^3) for each mirror. However, recall from the discussion of the second-order astigmatic-like terms (vis., N_{112}, N_{211}, and N_{222}), that the image plane tilt is an effective degree of freedom that can be used to eliminate N_{211} and N_{222} provided that N_{211} and N_{222} are equal. Therefore, in a two-mirror system, there are enough degrees of freedom from the two $C_{2,1}$ and $C_{0,3}$ (in which the aberration coefficients are linear) to control the terms that are independent of field (B_{112} and B_{222}), and to ensure that N_{112} is zero and N_{211} and N_{222} are equal. If the image plane tilt is also included as a degree of freedom, then all of the blur terms through second-order can be controlled. However, this leaves no additional degrees of freedom in which the distortion terms are linear, so nonlinear variables such as mirror tilts and separations need to be used if controlling distortion is important.

For the three-mirror Sample System used in this paper, if we include the image plane tilt, there are seven degrees of freedom for which the second-order coefficients are linear, but there are a total of eight coefficients (B_{112}, B_{222}, N_{112}, N_{211}, N_{222}, L_{112}, L_{211}, and L_{222}). This is why there was difficulty correcting all of the blur terms as well as the distortion in Section 4C when only the aspheric coefficients of the mirrors were allowed to vary. The system needed the extra degrees of freedom that come from changing the mirror tilts and separations to allow all of the blur terms as well as the distortion to be controlled.

REFERENCES AND REMARKS

[1] See, for example, industry news services such as http://spacenews.com/tag/smallsats/
[2] Beginning in October 2013, NASA started a new CubeSat Initiative to develop low cost options to enable scientific discovery. More can be found at: https://www.nasa.gov/content/goddard/nasas-science-mission-directorate-cubesat-initiative
[3] Bryan D. Stone and G. W. Forbes, "Foundations of first-order layout for asymmetric systems: an application of Hamilton's methods," J. Opt. Soc. Am. A 9, 96-109 (1992).
[4] Bryan D. Stone and G. W. Forbes, "Foundations of second-order layout for asymmetric systems," J. Opt. Soc. Am. A 9, 2067-2082 (1992).
[5] Bryan D. Stone and G. W. Forbes, "Illustration of second-order design methods: global merit function plots for a class of projection systems," J. Opt. Soc. Am. A 11, 3308-3321 (1994).
[6] Joseph M. Howard and Bryan D. Stone, "Anamorphic imaging with three mirrors: a survey," Proc. SPIE 7652, International Optical Design Conference 2010, 76520K (September 07, 2010).
[7] See, for example, W.T. Welford, *Aberrations of Optical Systems*, Bristol: Adam Hilger, Chapt. 7, 1986.
[8] Following [4], the first subscript of N_{ijk} indicates the field dependence: h_x for i=1 or h_y for i=2. The second two subscripts indicate the pupil dependence. For the terms in L, the last subscript of L_{ijk} indicates the pupil dependence: ρ_x for k=1 or ρ_y for k=2, and the first two subscripts indicate the field dependence.
[9] Synopsys, Inc., CODE V, Version 10.8, Mountain View, CA (2016).
[10] G. W. Forbes, "Characterizing the shape of freeform optics," Opt. Express, vol. 20, 2483-2499 (2012).